HYPERSPECTRAL FLUORESCENCE REMOTE SENSING OF LANDSCAPE MOLECULAR PROBES

John Anderson, Richard Massaro, Jarrod Edwards, Garry Glaspell
US Army Engineer Research and Development Center TEC
Fluorescence Lab, Alexandria, Virginia 22315
John.anderson@usace.army.mil

William Bernard, Oliver Weatherbee
SpectIR Corp.
8626 Brooks Dr. Ste. 103
Easton, Maryland 21601

ABSTRACT

Synoptic remote sensing of chemical, biological and radiological materials or targets using hyperspectral reflectance alone falls far short of material detection specificity. To enhance specificity for target confirmation, a fusion between fluorescence and hyperspectral reflectance sensing should permit more specific identifications of threats. To study the application of such a fusion technology, we have designed and tested a variety of high quantum yield molecular probes or "reporters" to work with molecular tags. This kind of remote sensing borrows heavily from molecular biology and uses the same "hair-pin" recognition and reporter constructs found in medical-clinical diagnostics. However, several important differences relate to the atmosphere, absorption cross-section and amount of suitable probe material for landscape-level sensing. To accomplish hyperspectral fluorescence sensing, we have demonstrated the recovery of probes illuminated by a third party laser and recorded by a hyperspectral scanner at night in darkfield. LIDAR equations were used to understand the target, excitation, source, sensor, and distance relationships. This paper will present these findings and discuss the potential benefits of such technology.

INTRODUCTION

Specificity in the remote sensing of biological, chemical and radiological threats can be challenging for reflectance-based multi- and hyperspectral systems. While spectral signatures for associated materials are valuable, they do not largely represent true molecular confirmation of actual agents or ancillary materials associated with defense or security threats. Still, much work is ongoing in refining high-resolution spectral reflectance-based sensors and algorithms to accomplish the detection of these materials for a variety of military operational and homeland security applications. As a compliment to high-resolution hyperspectral sensing technology, we have been actively investigating the use of companion fluorescence probes and taggants to provide a versatile and expanded resolution of information with regards to such targets. Molecular fluorescence is defined as the emission of a photon (typically at longer wavelengths), subsequent to the absorption of a photon (typically at a shorter wavelength) and involves selective wavelength absorption of a total spectrum or an external, coherent illumination source. In the past two decades, excellent examples of fluorescence remote sensing can be drawn from the plant / vegetative stress literature (Johansson, 1996; Lichtenthaler, 1996). Using plant sentinels and laser-induced fluorescence to explore the detection of natural and anthropogenic stress has been well documented. Recently, the use of genetically-programmed (plant and microbial) sentinels designed to express known fluorescence under specific excitation has also been reported (Stewart, 2005; Smirnova et al., 2004).

Borrowing from (and scaling up) clinical applications in molecular biology and analytical chemistry, photo-luminescent reporters appear to hold promise in the synoptic detection of environmental toxins, defense and security threats or their ancillary constituents. We have recently demonstrated the use of molecular sensors conjugated to high-quantum yield fluorescent reporters for stand-off and synoptic biological and chemical detection (Anderson, 2004; Anderson, 2002; Pestov, 2006; Pestov, 2004). In each case these sensors were used to directly detect directly an agent of interest or ancillary markers associated with the dispersal of a specific target material. Typically, these molecular reporters are introduced en masse into the environment and function as "hair-pin" recognition systems, thus binding with a specific target. Once the sensor and target are bound, the conjugated reporter fluorophore is released through competitive binding and is subsequently available for excitation. We have experimented with a

wide variety of organic and inorganic optical reporter constructs conjugated to molecular recognition systems and discovered that to accomplish terrestrial scale remote sensing, photo-luminescent reporters need to be robust, possess long decays (microsecond to millisecond) and have high quantum efficiencies (*QE* >0.5). Once activated "bistatically" by air or ground laser, emissions from materials with these characteristics are more than adequate to be detected by a scanner with variable integration timing. Until recently, this kind of remote sensing was limited to unique, "one-off," and proprietary experimental systems. For the first time, we report a recent experiment using a commercially-available hyperspectral scanner used to observe the emission of a high quantum yield target illuminated by stand-off laser at night in darkfield.

METHODS

Study Site

This experiment was conducted at Fort A.P. Hill, Virginia at a target farm we established in the southeastern section of the military base (map coordinates N38° 5.424' and W77° 20.209') southwest of the town of Baylorsville, Caroline County, Virginia, USA. Targets (black trays) approximately 1 m^2 in area and 3 cm in depth were placed in a large open field adjacent to a nearby road (figure 1). Each target was evenly coated with a rare earth-based down-converting photoluminescent material. Down-converting material is characterized by absorption of short wavelength light (e.g.,ultraviolet) and subsequent emission at longer wavelengths.

Figure 1. (left) Laser targets at the study site and

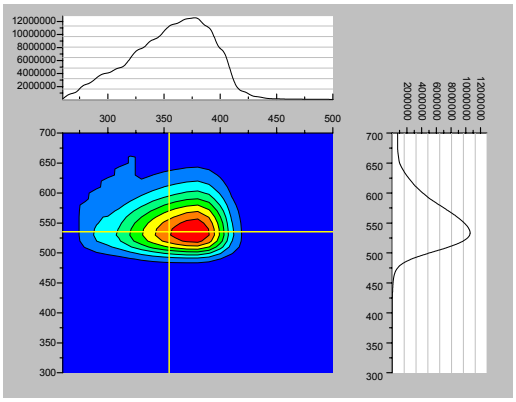

Figure 2 (right) total luminescence spectrum for reporter material.

UV Fluorescent Reporter

The reporter-target we tested was acquired from a collaborating, proprietary source. In general, this particular rare-earth based formulary contains composite Neodynum (Nd) and Yttrium (Yt) elemental fractions possessing a 370 nm absorption maxima (excitation by ultraviolet light). This is largely characteristic for many periodic lanthanide series materials. The synthesis and remote sensing of rare earth oxides are a leading research objective in our lab and using their electron transitions effectively in material compositions provides a multitude of emission qualities chemically tunable to a full spectrum of colors including pure red, green, blue and more recently white (Glaspell et al. in review). A total luminescence spectrum for the target material is shown in figure 2. It was determined that the material possessed a QE of 0.8 at an excitation of 355 nm. Approximately 0.25 Kg of material was distributed as a dry powder over the surface of 1 m^2 black tray at a thickness of 1 to 1.5 cm.

LIDAR Modeling (FLIMOD)

Fluorescence LIDAR calculations were used in order to simulate the integrated darkfield image taken by the high-resolution, hyperspectral airborne sensor. The image simulation is a fluorescence intensity image model, or FLIMOD (Massaro, unpublished data). The model estimates the ground sample distance (GSD) in meters per pixel by the similar triangle relationship,

EQ 1. $$gsd = R_{rec}\left(\frac{d_{pixel}}{f}\right)$$

where d_{pixel} is the size of an individual pixel within the CCD camera, f is the focal length of the receiver's optics, and R_{rec} is the receiver's height above the target. The illumination radius, r_{illum}, of the laser projected on the ground can be solved by,

EQ 2. $$r_{illum} = R_{laser}\tan\left(\frac{\theta_{div}}{2}\right) + \frac{d_{laser}}{2}$$

where R_{laser} is the laser distance from the target, θ_{div} is the laser beam's divergence angle, and d_{laser} is the intial diameter of the laser beam. The illumination radius on the ground in pixels is simply solved by dividing r_{illum} by the GSD and rounding off to the nearest pixel value. Two matrices, T and I, stand for target and illuminated pixels, respectively. The sizes of T and I are determined by the given CCD's height and width in pixels. Within the simulated image, the pixels which are mapped to the target are given a value of 1 and those that are not are given a value of 0. Similarly, pixels which are mapped to areas illuminated by the laser beam are given a value of 1 while those that are not laser illuminated are given a value of 0. The ambient flux, F_a, in $W/m^2/nm$ is a user-provided input and contributes to the background noise. It is assumed that the ambient flux is the same on all areas of the image. The energy emanating from a pixel due to the ambient flux is then,

EQ 3. $$E_{pixel} = \alpha F_a t_{\text{int}} gsd^2$$

where α is the surface albedo and t_{int} is the receiver's integration time. The units of E_{pixel} are $J/pixel^2/nm$. E_{pixel} is multiplied by a Gaussian white noise image with mean value of 1.0 to arrive at the background image, I_{BG}. The laser flux, F_L, in units of $J/pixel^2/nm/s$, is determined by,

EQ 4. $$F_L = \frac{E_L \nu_L}{\pi r_{illum}^2} gsd^2$$

where E_L is the laser energy per pulse and ν_L is the repetition rate of the laser. The fluorescence peak, F_0, after each laser pulse can then be defined as,

EQ 5. $$F_0 = F_L \eta_{atm} \eta_{abs} \eta_{QY} \eta_{rec}$$

where η_{atm} is the fraction of radiation transmitted through the atmosphere, η_{abs} is the fraction of laser light absorbed by the target, η_{QY} is the quantum yield of the target, and η_{rec} is the fraction of fluorescence radiation that is transmitted through the receiver's components. The total fluorescence intensity is found by summing the fluorescence of each pulse within the integration timeframe,

EQ 6. $$F_t = F_0\left[\int_{t=0}^{t_1} e^{\frac{-t}{\tau}}dt + \int_{t_1}^{t_2} e^{\frac{-t}{\tau}}dt + \ldots + \int_{t_n}^{t_f} e^{\frac{-t}{\tau}}dt\right]$$

where τ is the first-order kinetics fluorescence lifetime of the target material. The limits of integration are the "time stamps" for the arrival of each laser pulse within the integration time. Finally, the total image, J, is calculated by,

EQ 7. $$\mathbf{J} = \mathbf{I}_{BG} + F_t(\mathbf{T}\cdot\mathbf{I})$$

where T·I is the element by element multiplication of T and I.

Laser-Induced Fluorescence

Excitation of the target fluorescent reporter was accomplished using a laser induced fluorescence imager (LIFI). The LIFI possess a tripled Nd:YAG laser (Big Sky Laser, Montana) and special optics by STL (Santa Barbara, CA) for consistent broad field illumination. The laser emits a pulsed (20 Hz) source at 355 nm producing approximately 5 mJ of energy. At 2 meters, the laser field was approximately 0.75 m^2 representing a 5 degree dispersion. While 355 nm is not the optimal absorption line for the material, it is close enough and falls within a broad absorption region and provided a very efficient pump. The geometry of the excitation and receiver configuration was computed for a distance of 2 meters to establish the minimum resolving power (in arcseconds). Finally, photon recovery from the fluorescent target to the hyperspectral scanner was modeled by solving equation 8 which considers the power on the target (W/m^2), absorption, quantum yield and detector efficiency, energy per photon flux (J/ photon), portion of emission received, and finally atmospheric absorption.

EQ 8.

$$F(z) = \left(\frac{P_{laser} f}{A_{target}}\right)\left(\eta_{abs}\eta_{QY}\eta_{\substack{detector \\ eff}}\right)\left(\frac{hc}{\lambda_{\substack{peak \\ em}}}\right)^{-1}\left(\frac{A_{rec}}{4\pi z^2}\right)e^{-\alpha_f z}$$

Hyperspectral Imaging and Spectral Processing

Hyperspectral imagery was provided by SpectIR, Corp. of Easton, Maryland. A night mission (1930 to 2000 hours local time) was designed and flown concurrent with the laser excitation of the target. The sensor was adjusted to an integration time to accommodate the long decay of the target (> 1mS) Hyperspectral data (3 to 5 nm resolution) was generated using ProSpecTIR-VS (450-2450 nm) hyperspectral imaging spectrometer. Hyperspectral imagery was collected from two east-to-west flight lines between 500 and 800 meters (AGL) providing data sets representing 0.3 – 0.5 meters / pixel on the ground and a final spectral cube 356 bands deep. These data were post-processed for geometric and radiometric effects. Spectral analysis on the final data set was performed using ENVI (RSI, Inc.) and Matrix Laboratory (the Math Works).

RESULTS

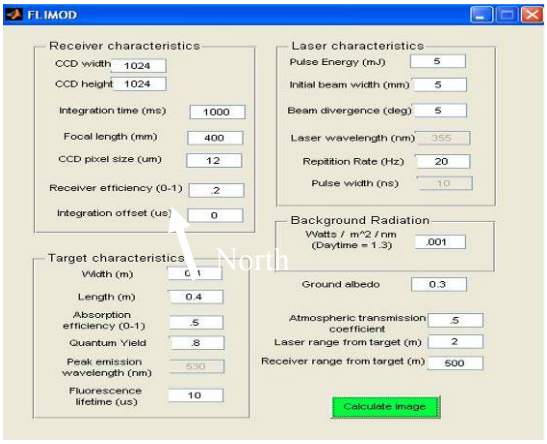

Figure 3. FLIMOD GUI and input parameters.

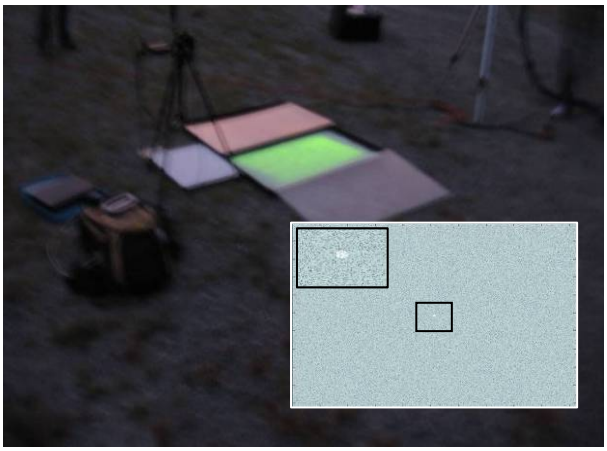

Figure 4. Target illuminated by LIFI and (inset) pixel prediction image results based on FLIMOD.

The graphical user interface (GUI) for FLIMOD is shown in Figure 3. The parameters match those of the experimental setup to determine the recovered pixels given the LIDAR parameters used. The simulated image for the parameters provided is shown in figure 4 (inset) and an enlarged view of the target fluorescence is shown in Figure 4. It was estimated that only 5 to 7 pixels within the image field would be detected by the hyperspectral scanner at an altitude of 500 to 800 meters.

An example of the illuminated target and concurrently acquired hyperspectral imagery are shown in figure 5. For spatial reference, the night mission data has been overlaid onto a base image of Fort A.P. Hill. The high

quantum yield of the target permitted 6 to 7 pixels to be measured within the 490 to 610 nm bandpass as calculated by the FLIMOD software. The resulting image-derived spectra also show good correlation with the emission characteristics of the target material characterized under UV excitation (see Figure2).

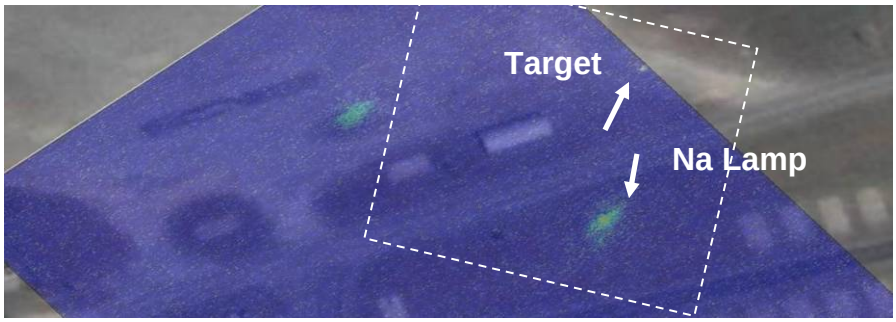

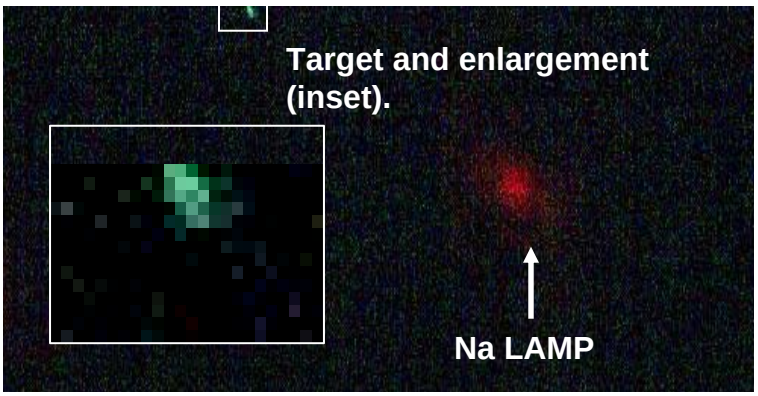

Figure 5. (Above) Image base over Ft. A.P. Hill overlaid with darkfield imagery showing position of sodium vapor lamps and target near scene edge (arrow).
Figure 5 (Below) Area within dashed line above representing SpectIR ProSpec hyperspectral data using bands 589, 550, 580 (RGB).

Figure 6 A presents a darkfield, reflectance-calibrated spectrum for the excited target collected for comparison to image-derived spectra using an ASD Full Range spectrometer (ASD, Bolder, CO). These data can be used to examine the structure of the image-derived spectra for the target. The target was best detected within the imagery from 500 nm to 610 nm as the ASD spectra suggest (area within solid box). Multiple emission peaks occur for the target within this range with a peak emission occurring at 550 nm (figure 6 B). Also observed in the image data are two sodium vapor lamps illuminating two parade fields adjacent to the target farm. These lamps (trending East to West along the flight line) served as excellent calibration sources with a strong (Na) spectral line measured at 589 - 590 nm (figure 6 C). The image spectra suggest a detected overlapping emission from stray photons between the nearby lamps and emitting target, but good and measureable separation for the targets is still accomplished. Furthermore, it would appear that bleed-over of photons from the lamps may have occurred since the Na line is also seen in the end structure of the target spectrum.

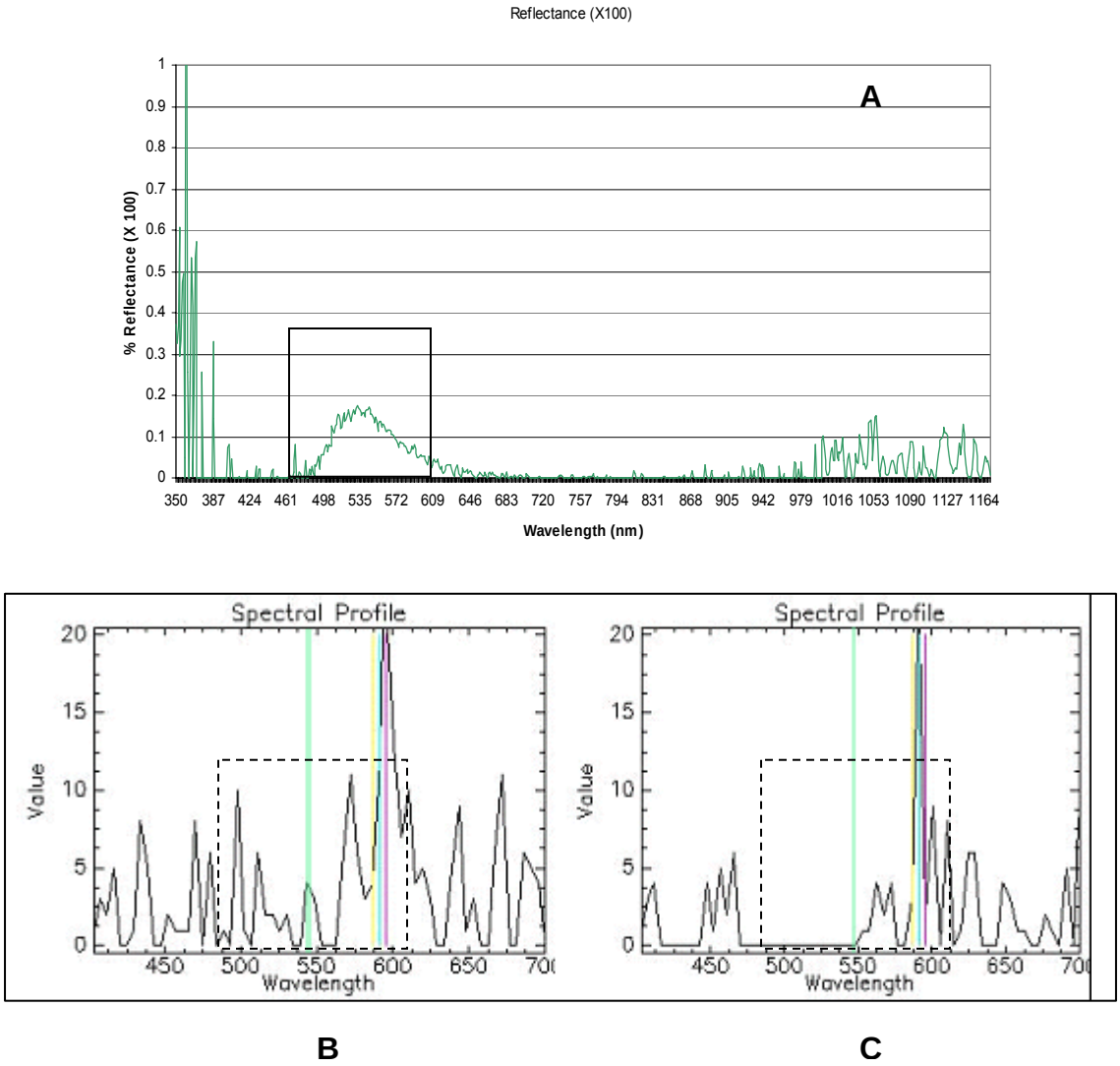

Figure 6 A . (Above) ASD darkfield spectrum for target under laser illumination.
Figure 6 B. (Lower Left) Image-derived spectrum for target showing populated pixels in the 490 to 610 nm bandpass (dashed box).
Figure 6 C. (Lower Right) Image-derived spectrum for Na lamps showing sharp peak at 589-590 nm.

We have demonstrated the recovery of a high quantum yield optical reporter material based upon a rare-earth formulary. The pre-mission modeling of laser-induced fluorescence and recovery by a commercial hyperspectral reflectance system showed that optical reporters can be distributed and imaged in darkfield. This is seen as a new frontier in remote sensing where molecular sensors conjugated to such reporters should provide another analytical resolution and make target confirmation a reality.

REFERENCES

Anderson, J., S. Webb, R. Fischer, C. Smith, J. Dennis, and J. Di Benedetto, 2001. In situ detection of the pathogen indicator e. coli using active laser-induced fluorescence imaging and defined substrate conversion, *Journal of Fluorescence,* 12, no. 1, 51-55.

Anderson, John, Jean Nelson, Charles Reynolds, Dave Ringelberg, Gary Tepper, and Dmitry Pestov, 2004. Steady-state and frequency-domain lifetime measurements of an activated molecular imprinted polymer imprinted to dipicolinic acid, *Journal of Fluorescence,* 14, no. 3, 269-274.

Cecchi, Giovanna, Marco Bazzani, Luca Pantani, Piero Mazzinghi, and Valentina Raimondi, 1995. Fluorescence LIDAR remote sensing of vegetation, *Proceedings of SPIE-The International Society for Optical Engineering,* 2585, no. Remote Sensing for Agriculture, Forestry, and Natural Resources, 48-56.

Chappelle, Emmett W., Lawrence A. Corp, James E. McMurtrey, Moon S. Kim, and Craig S. T. Daughtry, 1997. Fluorescence: A diagnostic tool for the detection of stress in plants, *Proceedings of SPIE-The International Society for Optical Engineering,* 2959, no. Remote Sensing of Vegetation and Sea, 14-23.

Chappelle, Emmett W., James E. McMurtrey, III, Frank M. Wood, Jr., and W. Wayne Newcomb, 1984. Laser-induced fluorescence of green plants. 2. Lif caused by nutrient deficiencies in corn, *Applied Optics,* 23, no. 1, 139-42.

Chappelle, Emmett W., Frank M. Wood, Jr., W. Wayne Newcomb, and James E. McMurtrey, III, 1985. Laser-induced fluorescence of green plants. 3: Lif spectral signatures of five major plant types, *Applied Optics,* 24, no. 1, 74-80.

Farley, Vincent, Alexandre Vallieres, Andre Villemaire, Martin Chamberland, Philippe Lagueux, and Jean Giroux, 2007. Chemical agent detection and identification with a hyperspectral imaging infrared sensor, *Proceedings of SPIE-The International Society for Optical Engineering,* 6739, no. Electro-Optical Remote Sensing, Detection, and Photonic Technologies and Their Applications, 673918/1-673918/12.

Farrell, Michael D., Jr., and Russell M. Mersereau, 2005. Detection of industrial gaseous chemical plumes using hyperspectral imagery in the rmissive tegime, *Proceedings of SPIE-The International Society for Optical Engineering,* 5890, no. Atmospheric and Environmental Remote Sensing Data Processing and Utilization: Numerical Atmospheric Prediction and Environmental Monitoring, 58900E/1-58900E/12.

Garry Glaspell , John Anderson, James Wilkins and M. Samy El-Shall. Vapor phase synthesis of upconverting Y2O3 nanocrystals doped with Yb^{3+}, Er^{3+}, Ho^{3+} and Tm^{3+} to generate red, green, blue and white light, *Journal of Physical Chemistry,* (Submitted Paper).

Gomez, Richard B., and Swarvanu Dasgupta, 2004. Use of hyperspectral remote sensing for detection and monitoring of chemical and biological agents - A survey, *Proceedings of SPIE-The International Society for Optical Engineering,* 5584, no. Chemical and Biological Standoff Detection II, 276-285.

Irina A. Smirnova, Cyril Dian, Gordon A. Leonard, Seán McSweeney, Darcy Birse and Peter Brzezinski, 2004. Development of a bacterial biosensor for nitrotoluenes: The crystal structure of the transcriptional regulator dntr , *Journal of Molecular Biology,* 340, no. 9, July 405-418.

Johansson, Jonas, Mats Andersson, Hans Edner, Johan Mattsson, and Sune Svanberg, 1996. Remote fluorescence measurements of vegetation spectrally resolved and by multi-color fluorescence imaging, *Journal of Plant Physiology,* 148, no. 5, 632-637.

Lichtenthaler, H. K., M. Lang, M. Sowinska, F. Heisel, and J. A. Miehe, 1996. Detection of vegetation stress via a new high resolution fluorescence imaging system, *Journal of Plant Physiology,* 148, no. 5, 599-612.

Manolakis, Dimitris, and Francis M. D'Amico, 2005. Design and evaluation of hyperspectral algorithms for chemical warfare agent detection, *Proceedings of SPIE-The International Society for Optical Engineering,* 5995, no. Chemical and Biological Standoff Detection III, 599503/1-599503/13.

Pestov, Dmitry, John E. Anderson, Jean Nelson, and Gary C. Tepper, 2004. Chemical point detection using differential fluorescence from molecularly imprinted polymers, *Proceedings of SPIE-The International Society for Optical Engineering,* 5585, no. Chemical and Biological Point Sensors for Homeland Defense II, 109-112.

Pestov, Dmitry, John Anderson, and Gary Tepper, 2006. Differential fluorescence from molecularly imprinted polymers containing europium ions as a transducer element, *Proceedings of SPIE-The International Society for Optical Engineering,* 6378, no. Chemical and Biological Sensors for Industrial and Environmental Monitoring II, 63780Y/1-63780Y/5.

Stewart, C. Neal, Jr., Reginald J. Millwood, Matthew D. Halfhill, Mentewab Ayalew, Vinitha Cardoza, Mitra Kooshki, Gene A. Capelle, Kevin R. Kyle, David Piaseki, Gregory McCrum, and John Di Benedetto, 2005. Laser-induced fluorescence imaging and spectroscopy of Gfp transgenic plants, *Journal of Fluorescence,* 15, no. 5, 697-705.

Vallieres, Alexandre, Andre Villemaire, Martin Chamberland, Louis Belhumeur, Vincent Farley, Jean Giroux, and Jean-Francois Legault, 2005. Algorithms for chemical detection, identification and quantification for

thermal hyperspectral imagers, *Proceedings of SPIE-The International Society for Optical Engineering*, 5995, no. Chemical and Biological Standoff Detection III, 59950G/1-59950G/11.